

Laboratory Astrophysics using a Spare XRS Microcalorimeter

*F. S. Porter, M. D. Audley, P. Beiersdorfer, K. R. Boyce,
R. P. Brekosky, G. V. Brown, K. C. Gendreau, J. Gygax,
S. Kahn, R. L. Kelley, C. K. Stahle, and A. E. Szymkowiak*

This article was submitted to
SPIE International Symposium on Optical Science and Technology
San Diego, CA
July 30 – August 4, 2000

U.S. Department of Energy

Lawrence
Livermore
National
Laboratory

August 7, 2000

DISCLAIMER

This document was prepared as an account of work sponsored by an agency of the United States Government. Neither the United States Government nor the University of California nor any of their employees, makes any warranty, express or implied, or assumes any legal liability or responsibility for the accuracy, completeness, or usefulness of any information, apparatus, product, or process disclosed, or represents that its use would not infringe privately owned rights. Reference herein to any specific commercial product, process, or service by trade name, trademark, manufacturer, or otherwise, does not necessarily constitute or imply its endorsement, recommendation, or favoring by the United States Government or the University of California. The views and opinions of authors expressed herein do not necessarily state or reflect those of the United States Government or the University of California, and shall not be used for advertising or product endorsement purposes.

This is a preprint of a paper intended for publication in a journal or proceedings. Since changes may be made before publication, this preprint is made available with the understanding that it will not be cited or reproduced without the permission of the author.

This report has been reproduced
directly from the best available copy.

Available to DOE and DOE contractors from the
Office of Scientific and Technical Information
P.O. Box 62, Oak Ridge, TN 37831
Prices available from (423) 576-8401
<http://apollo.osti.gov/bridge/>

Available to the public from the
National Technical Information Service
U.S. Department of Commerce
5285 Port Royal Rd.,
Springfield, VA 22161
<http://www.ntis.gov/>

OR

Lawrence Livermore National Laboratory
Technical Information Department's Digital Library
<http://www.llnl.gov/tid/Library.html>

Laboratory Astrophysics using a Spare XRS Microcalorimeter

F. Scott Porter^a, M. Damian Audley^b, Peter Beiersdorfer^c, Kevin R. Boyce^a, Regis P. Brekosky^{a,d}, Gregory V. Brown^c, Keith C. Gendreau^a, John Gygax^{a,d}, Steven Kahn^c, Richard L. Kelley^a, Caroline K. Stahle^a, Andrew E. Szymkowiak^a

^aNASA/Goddard Space Flight Center, Greenbelt, MD

^bInstitute of Space and Astronautical Science, Sagami-hara, Japan

^cLawrence Livermore National Laboratory, Livermore, CA

^dSwales and Associates, Beltsville, MD

^eColumbia University, New York, NY

ABSTRACT

The XRS instrument on Astro-E is a fully self-contained microcalorimeter x-ray instrument capable of acquiring, optimally filtering, and characterizing events for 32 independent pixels. We have recently integrated a full engineering model XRS detector system into a laboratory cryostat for use on the electron beam ion trap (EBIT) at Lawrence Livermore National Laboratory. The detector system contains a microcalorimeter array with 32 instrumented pixels heat sunk to 60 mK using an adiabatic demagnetization refrigerator. The instrument has a composite resolution of 8 eV at 1 keV and 11 eV at 6 keV with a minimum of 98% quantum efficiency and a total collecting area of 13 mm². This will allow high spectral resolution, broadband observations of plasmas with known ionization states that are produced in the EBIT experiment. Unique to our instrument are exceptionally well characterized 1000 Angstrom thick aluminum on polyimide infrared blocking filters. The detailed transmission function including the edge fine structure of these filters has been measured in our laboratory using a variable spaced grating spectrometer. This will allow the instrument to perform the first broadband absolute flux measurements with the EBIT instrument. The instrument performance as well as the results of preliminary measurements of Fe K and L shell at fixed electron energy, Fe emission with Maxwellian electron distributions, and phase resolved spectroscopy of ionizing plasmas will be discussed.

Keywords: X-ray, Laboratory Astrophysics, Cryogenic Detector

1. INTRODUCTION

X-ray astronomy is a very rich field for studying astrophysical phenomena. Plasmas surrounding active galactic nuclei, in supernova remnants, and in galaxy clusters, for example, emit radiation predominately in the x-ray. The x-ray emission from these objects can give key insights into the local conditions where the x-rays are produced including the ionization state of the plasma, the ionization equilibrium, and the composition of the plasma. Since 1992, the ASCA satellite has surveyed hundreds of objects providing moderate resolution spectra using its two CCD cameras. The current state of the spectroscopic models, including the MeKaL code is sufficient to model many of the results. However, even with ASCA, the existing models can sometimes give misleading results. With the launch of Chandra and XMM and their high resolution grating spectrometers, the situation becomes much more complicated. The grating instruments on these satellites are capable of observing line ratios of closely spaced emission lines, including Fe L shell lines from various ionization states of Fe, an important tracer of hot astrophysical plasmas. With these data, the details of the atomic physics models are becoming extremely important including exact line positions for each ionization state, and their relative cross-sections as a function of electron temperature. In addition, many systems including supernova remnants are not in thermodynamic equilibrium further complicating the interpretation.

In addition to Chandra and XMM there was to be a third observatory, Astro-E, with the ability to do high resolution x-ray spectroscopy. Unfortunately, earlier this year, the satellite failed to reach orbit. The Astro-E satellite included a novel high resolution x-ray spectrometer, the XRS, based on a cryogenic microcalorimeter array¹ composed of a 32 segment pixilated detector described more completely in section 2. The microcalorimeter had a resolution of 8 eV at 1.5 keV and 11 eV at 6 keV and had more collecting area than Chandra and XMM at the important Fe K emission region near 6 keV. It also had a

^{*}Correspondence: Email: Frederick.S.Porter@gsfsc.nasa.gov; WWW: <http://phonon.gsfsc.nasa.gov>; Telephone: 301-286-5016

broad bandpass extending from 0.3 keV through 12 keV. Since the detector was non-dispersive, it was well suited for looking at extended objects, which can be difficult with the grating instruments. Thus the XRS on Astro-E would have complemented well the instruments on the other two satellites.

With the Astro-E program, we built a complete working engineering model detector assembly and read-out electronics as well as the flight system and a flight spare. With the loss of Astro-E, the flight spares have been placed in storage to await a possible Astro-E reflight or a reduced scope small explorer mission. However, this left the engineering model detector system available for laboratory use. We have recently integrated the detector assembly module and a 32 element flight-like detector array into a laboratory cryostat for use with the Electron Beam Ion Trap (EBIT) at Lawrence Livermore National Laboratory (hereafter referred to as the XRS/EBIT). The beauty of using an XRS engineering model in the laboratory is that it has self contained read-out and front end processing for the full 32 channels, including pulse height and pulse shape analysis, 10 us pulse timing, pile-up detection, and noise analysis. This greatly simplifies our ability to field a multi-channel microcalorimeter instrument for laboratory use.

The EBIT machine is arguably the best ion source yet constructed for studying astrophysically interesting plasmas on the ground^{2,3}. The EBIT at LLNL can inject both gases and metals and form collisionally excited plasmas with electron densities of about $10^{12}/\text{cm}^3$. In addition, the EBIT produces nearly pure ionization states because of its monoenergetic electron beam that both ionizes and excites the target plasma. The EBIT can then approximate a plasma in thermodynamic equilibrium by sweeping the electron beam energy to produce a Maxwellian distribution at a given temperature⁴. The combination of these two modes, monoenergetic and Maxwellian, allows us to do detailed emission line surveys of astrophysically interesting plasmas from direct excitation, radiative recombination, and dielectronic recombination.

Using the EBIT machine and reflection grating spectrometers, the L shell emission from Fe has been mapped for various charge states including XVIII-XXIV^{5,6} with resolving powers of about 1000 at 1 keV. While this is almost 10 times better than the resolution of the XRS microcalorimeter at the same energies, the XRS/EBIT has a great deal to offer as a complement to the grating spectrometer. The high quantum efficiency (95% at 6 keV), and relatively large collecting area (13 mm^2) of the XRS/EBIT along with its large bandpass (0.1 — >12 keV in its laboratory configuration) make it an extremely fast detector allowing many observations to be completed in a short amount of time. In addition, the response function of the XRS/EBIT has been well characterized (see section 2) allowing precise measurements of line flux ratios, which are difficult to achieve with the grating instruments. Finally, the XRS/EBIT is insensitive to the individual polarization components. This helps in the interpretation of the high resolution crystal spectra which typically preferentially reflect one polarization component.

The XRS/EBIT system was installed on the EBIT machine on July 19, 2000 and has been continuously taking data, except for cryogenic servicing, for several weeks. We present some of these results in Section 3. The results presented are to demonstrate the operational capabilities of the XRS/EBIT system and are preliminary, meaning that the analysis has not yet been completed. In our early experiments, we have concentrated on Fe K and L shell emission at fixed electron energy, radiative recombination, and maxwellian distributions of electron energy with $\langle kT \rangle$ between 0.5 and 3 keV. Finally, we have used the exceptional timing capabilities of the XRS together with a GPS based timing synchronization system to perform phased resolved spectroscopy with the EBIT injection cycle. This allows us to look in detail at non-equilibrium plasmas that are charging up from the low charge state when the ions are injected into the electron beam until they reach ionization equilibrium. We have taken many hours of phase folded data and have observed time slices of 5 ms with excellent statistics.

The long term goal of using the XRS/EBIT, grating spectrometers and the EBIT machine is to provide maps for interpreting the high resolution spectra obtained by Chandra, XMM, and in the future an XRS-like instrument and Constellation-X. We hope to provide detailed and precise line ratio maps of highly ionized charge states of abundant astrophysical elements from oxygen to iron. In addition we hope to provide precise demonstrations of line ratios in non-equilibrium plasmas and collisionally excited thermal plasmas at a range of electron temperatures.

2. EXPERIMENTAL SETUP

In this section we will describe the XRS/EBIT instrument and the EBIT machine from the bottom up, so to speak, starting with the microcalorimeter detector and moving through the EBIT machine itself. Finally we will describe the current configuration of the XRS/EBIT-EBIT experiment.

2.1 The XRS/EBIT microcalorimeter detector

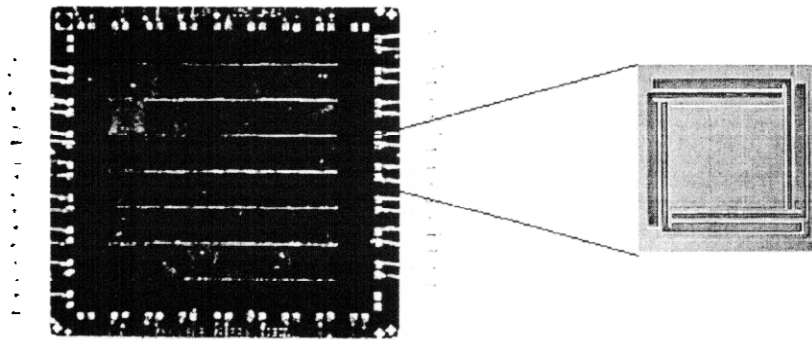


Figure 1. The XRS/EBIT 6x6 microcalorimeter array. The blowup on the right is a single pixel before the HgTe absorber has been attached, showing the thermal isolation beams.

Microcalorimeter x-ray detectors function by measuring the heat input for a single x-ray absorbed into a thermally isolated structure with a very sensitive thermometer (for an extensive discussion see Stahle et al.⁷). The XRS/EBIT detectors use an ion-implanted thermistor with very high sensitivity near the 0.06 K operating point of the detector. The XRS/EBIT microcalorimeter array, shown in Figure 1, is composed of 36 pixels on a 0.64 mm grid in a 6x6 configuration. The pixels are micromachined out of a single piece of silicon and are ion implanted to form Mott hopping conductivity thermistors on each suspended island. Thermal isolation is achieved by thinning the pin-wheel support legs to $\sim 8 \mu\text{m}$ thickness. Thus the entire array structure can be monolithically produced using standard microelectronics techniques⁸. The x-ray absorbing material is HgTe that is epitaxially grown on a CdZnTe/CdTe substrate and then diced into single x-ray absorbers which are carefully attached with a spacer to each detector in the array with a small dot of epoxy. The absorbers overhang the legs and frame structure of each pixel to give a 95% close packing fraction and an effective area of $0.41 \text{ mm}^2/\text{pixel}$. The choice of HgTe as an absorbing material is a compromise between fast thermalization and minimum heat capacity. We have successfully used this absorber material in both our XRS flight program and our XQC sounding rocket with thickness between 1 and $10 \mu\text{m}$. The XRS/EBIT detector has $8.5 \mu\text{m}$ thick HgTe absorbers giving us a minimum of 95% quantum efficiency through 6 keV and 67% at 10 keV. The energy resolution of the detector with all 32 pixels co-added is 8 eV at 1 keV and 11 eV at 6 keV.

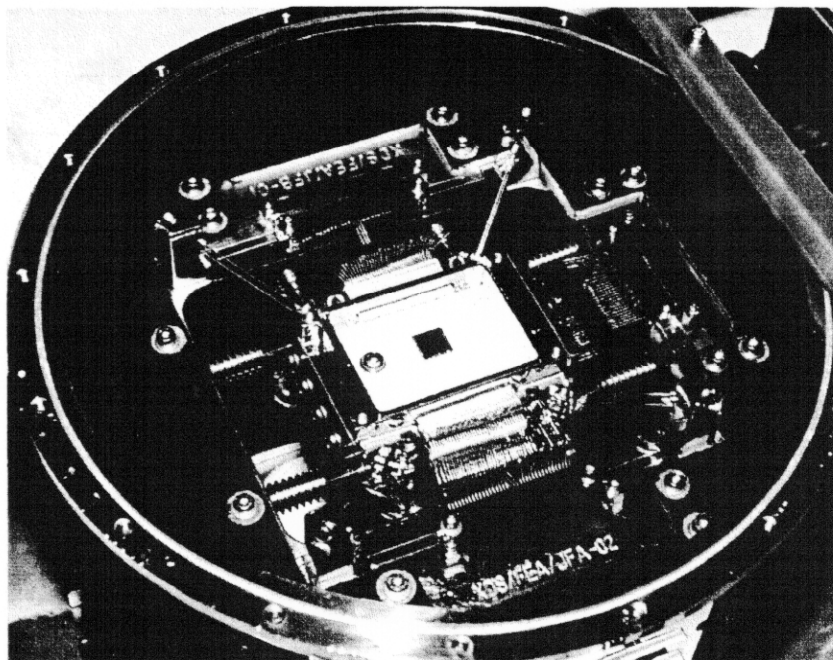


Figure 2. A closeup of the top of the detector front end assembly (FEA). The XRS/EBIT microcalorimeter array is centered in the picture.

The 6x6 detector array was originally selected for flight in the XRS instrument and underwent an extensive six week calibration program including mapping spectral redistribution and the resolution core as a function of energy using high performance monochrometers. However, late in the program, a subtle thermal mechanical failure in the 6x6 detector due to its mechanical support was uncovered and the 6x6 configuration was replaced for flight by an older and more robust 2x18 configuration. The 6x6 used in the XRS/EBIT detector is the same array that was originally scheduled to fly in XRS. The array had 4 broken pixels do to thermal mechanical stress but since the XRS has only 32 readout channels we were able to replace the broken pixels with the spares on the corners of the 36 pixel array. We then implemented a less constrained mounting scheme for the XRS/EBIT and the system appears to be very robust. Thus we are able to leverage our current experiments off of the extensive original XRS calibration program.

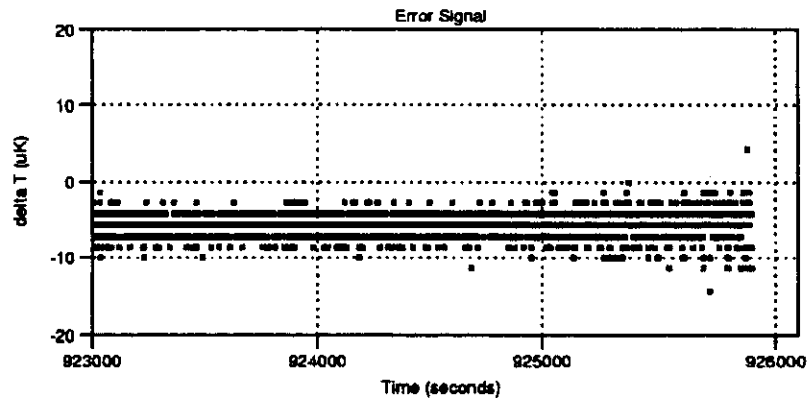


Figure 3. The error signal of the control thermometer for the XRS/EBIT ADR at 59 mK. The error signal is $< 5 \mu\text{K}$ RMS, and $5 \mu\text{K}$ D.C. from the set point temperature. A 3000 second time sequence is shown.

We have mounted the XRS/EBIT detector array in an XRS engineering model front end assembly (FEA) which is a modular structure mounted on the helium reservoir in the cryostat. The FEA contains the Kevlar isolation for the 60 mK detector stage, infrared blocking filters and 32 FET readout channels. The thermistors for each channel are read out in a voltage divider arrangement with a $90 \text{ M}\Omega$ load resistor by a FET source follower cooled to 130 K. The temperature controlled FET stages, and their suspension structure to provide thermal isolation from the helium tank are all integrated into the FEA. A picture of the FEA with its covers removed is shown in Figure 2. The modular nature of the FEA greatly simplified its integration into the XRS/EBIT cryostat.

2.2 The XRS/EBIT cryostat

The XRS flight instrument used a 32 liter superfluid helium tank at 1.3 K coupled to a solid neon outer cryogen tank at 17 K giving a two year cryogen lifetime. The low temperature refrigerator⁹ on the XRS was an adiabatic demagnetization refrigerator (ADR) using 1 kg of FAA refrigerant. Such a complex, expensive, and large arrangement is not practical in the laboratory, especially with the desire to minimize the distance between the EBIT machine and the detector. Thus we adapted a standard laboratory liquid helium cryostat to accept a smaller 50 g ADR developed for our XQC sounding rocket program. The resultant cryostat accepts the XRS detector assembly axially and looks out the bottom of the cryostat. By manufacturing the cryostat with offset cryogen ports we are able to successfully operate and fill cryogens in the experiment while it is operated horizontally. In this configuration the liquid helium bath is pumped to 1.5 K and has a 36-48 hour hold time on ~ 6 liters of helium. The 50 g ADR has typically run for ~ 12 hours at 59 mK with $0.7 \mu\text{W}$ of parasitic heat load. However, due to a structural imperfection in the salt pill housing, its performance is currently 5.5 hours at 59 mK. This will be corrected in the next build of the cryostat.

Temperature control of the detector assembly is achieved using commercial doped germanium thermometers readout by a high performance resistance bridge and a software PID controller fed back to the superconducting magnet that controls the temperature of the ADR. This arrangement is simple, robust, and requires no custom hardware. We consistently achieve temperature control of $< 5 \mu\text{K}$ RMS at 60 mK as shown in Figure 3. The limitation is currently the resolution of our AVS-47 resistance bridge since we are currently controlling to within 2 or 3 LSBs of the readout.

The XRS/EBIT cryostat includes four 1000 Å thick polyimid infrared blocking filters with between 400-1000 Å of aluminum each. These are necessary to eliminate excessive heating of the detector and the refrigerator from the 300K external port and to eliminate photon shot noise from visible photons. The filters used are left over from the XRS program and have not been optimized for use with the EBIT. Parylene filters with less aluminum as used successfully in our sounding rocket program may be more appropriate for this application and will be investigated for future use. Finally there is a 1 μm thick Be window on the main shell of the cryostat to isolate the dewar vacuum from the EBIT vacuum. The detailed response function of these filters as a function of x-ray energy is of primary importance for doing any sort of absolute flux measurements with this instrument and will be discussed in section 3.

2.3 Detector Readout electronics

Another benefit from utilizing technology developed during the XRS program is that the room temperature readout electronics is complete, modular, and extremely powerful. The XRS/EBIT instrument contains a full set of XRS engineering model room temperature electronics. This system includes preamplifiers, anti-aliasing filters, ADCs, and a complete digital analysis chain for each channel along with extensive housekeeping functions. The digital analysis chain consists of a high performance DSP for each channel that generates and then applies an optimal filter matched to the x-ray pulse shape and the noise environment. An extensive description of the digital electronics is given in Boyce et al.¹⁰ The output of the digital electronics chain is a 64 bit descriptor for each x-ray event giving its optimally filtered pulse height, risetime, flags, and a 10 us resolution time stamp. Other functions include pile-up detection, the collection of noise spectra, and IV curves for the individual channels. Finally the analog chain provides automatic control over the 32 FET source follower channels and controls the anti-coincidence detector which is stationed beneath the detector array. The use of the XRS electronics system greatly accelerated our ability to field a 32 channel instrument for use with the EBIT facility.

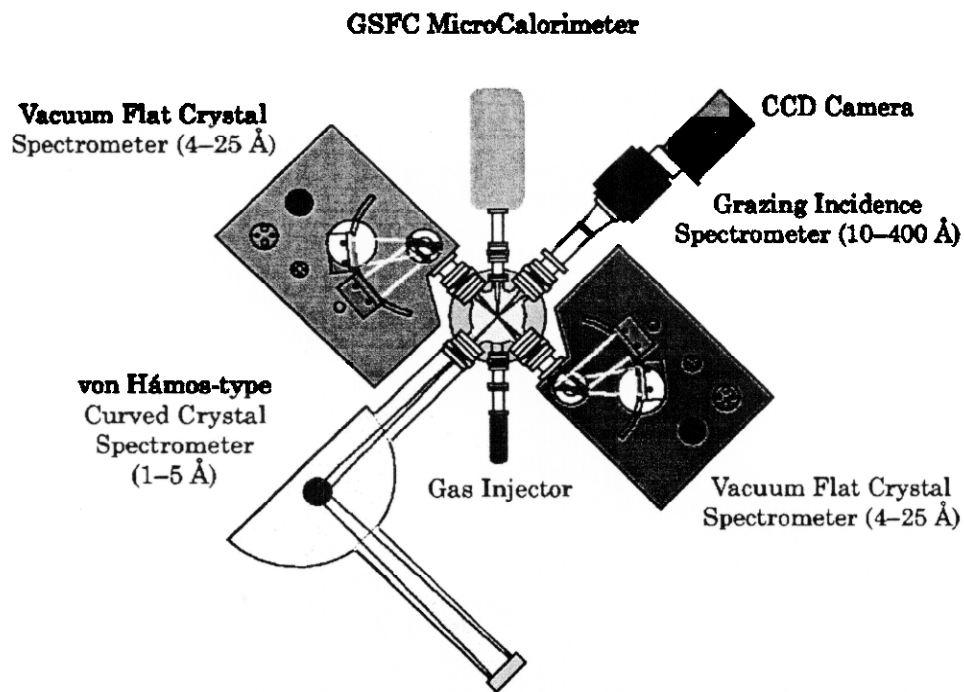


Figure 4. Current configuration of the EBIT machine with the XRS/EBIT microcalorimeter detector at the top of the figure.

Pulse time tagging is extremely important for operation with the EBIT. The EBIT machine performs a periodic cycle of ion injection, trapping, and dumping of the trapped ions. The cycle time is typically a few seconds. In order to avoid, or to specifically observe, the non-equilibrium charge state distributions right after injection, it is necessary to time tag the x-ray events in the detector with respect to the EBIT cycle time. We achieve this using a commercial GPS time synchronization system that correlates time pulses from our detector electronics with cycle initiation pulses from the EBIT machine. We are then able to assign a phase time to each x-ray event. The event file is then phase folded on the injection time and the regions of interest extracted. This is a very powerful technique for looking at non-equilibrium ionization states as discussed in section 4.

2.4 The Electron Beam Ion Trap (EBIT)

The electron beam ion trap was designed and implemented at the Lawrence Livermore National Laboratory. It was specifically developed and built for studying the interactions of electrons with highly charged ions using X-ray spectroscopy¹¹. Neutral atoms or ions with low charge are injected into a nearly monoenergetic beam where they are collisionally ionized and excited by an electron beam. The beam electrons are confined and focused by a 3 Tesla magnetic field, generated by a pair of superconducting Helmholtz coils. As the beam passes through the trap region of 2-cm length, it is compressed to a diameter of approximately 60 μm . Ions are longitudinally confined in the trap by applying the appropriate voltages to a set of three drift tubes through which the beam passes. Radial confinement is provided by electrostatic attraction of the electron beam, as well as flux freezing of the ions within the magnetic field. All three drift tube voltages float on top of a common potential that is supplied by a fast-switching high-voltage amplifier. The electron beam energy is determined by the sum of these potentials and may range between about 150 and 20,000 eV for most measurements of interest. The electron beam density at a given beam energy can be selected by varying the beam current. It typically is in the range of $2 \times 10^{11} - 5 \times 10^{12} \text{ cm}^{-3}$.

Six axial slots cut in the drift tubes and aligned with six vacuum ports permit direct line-of-sight access to the trap. One port is used for introducing atomic or molecular gases into the trap by means of a ballistic gas injection system. The remaining five ports are used for spectroscopic measurements, including the XRS/EBIT detector system. A seventh port on top of EBIT permits axial access to the trap and is used for the injection of singly charged metal ions in the trap from a metal vapor vacuum source.

2.5 The XRS/EBIT detector coupled to the EBIT machine at LLNL

The XRS/EBIT detector is attached to one of six radial ports on the EBIT machine as shown in Figure 4. The distance between the detector and the ion trap is less than 60 cm in its current configuration. This gives a count rate of between 50 and 300 counts/second/array for the experiments we have performed to date. This is well matched to the capabilities of the XRS/EBIT system, which runs efficiently at rates up to about 300 cps/array.

With the XRS/EBIT running horizontally we obscure only one of six ports of the EBIT machine allowing other spectrometers to be used simultaneously with the calorimeter. Currently we are using three vacuum flat crystal spectrometers¹², one or two von Hamos curved crystal spectrometers¹³, a flat-field grating spectrometer¹⁴ or a germanium detector and the XRS/EBIT for both broad band and high spectral resolution coverage. This is essential since the crystal spectrometers with resolutions of about 1 eV FWHM can resolve the line blends in the calorimeter, which adds broad band coverage and higher statistics.

The XRS/EBIT detector system after a week of assembly and calibration spot checks was attached to the LLNL EBIT machine on July 19, 2000. At the time of this writing it has been successfully operating for two weeks on a 24 hour, 7 day a week schedule except for cryogen servicing.

3. CALIBRATION

Calibration of the detector system is a multi-phase, time-consuming, but extremely important component for doing laboratory astrophysics. The XRS/EBIT detector is very complex which makes this task all the more important. From the XRS program we inherited measurements of the resolution core and spectral redistribution in the detector as a function of energy¹⁵ performed with high resolution x-ray monochrometers. Spot checks of these measurements in the current configuration have shown that the detectors have not changed since that time. In addition however, the energy scale of the detectors must be known with high precision over the entire bandpass. The energy scale calibration at high energies was done by using a rotating target fluorescence wheel excited by an x-ray tube. The results of this measurement are shown in Figure 5. The low energy calibration was done with the EBIT itself by using the known position of O, Fe and Ar K and L shell emission.

Of crucial importance in doing absolute flux studies at EBIT over a broad bandpass is to know the precise transmission function of the filter stack. This is a two fold process of measuring the Al and O K edge structure in an external apparatus and then measuring any contribution from ice accumulated on the filters in-situ after the experiment is cooled down. The ice measurement must then be repeated periodically to track any changes in the ice thickness. For the external calibration, we inserted the filter stack into a variable spaced grating spectrometer equipped with an x-ray CCD camera. The grating allowed us to measure the O and Al edge structure with a broadband x-ray beam without scanning the spectrometer. The filters were

then periodically inserted and removed to do an A-B measurement on the CCD detector. This is the same procedure utilized for the XRS flight filter stack¹⁶. The filters currently in the XRS/EBIT instrument were calibrated for approximately 4 weeks using this method with the results shown in Figure 6.

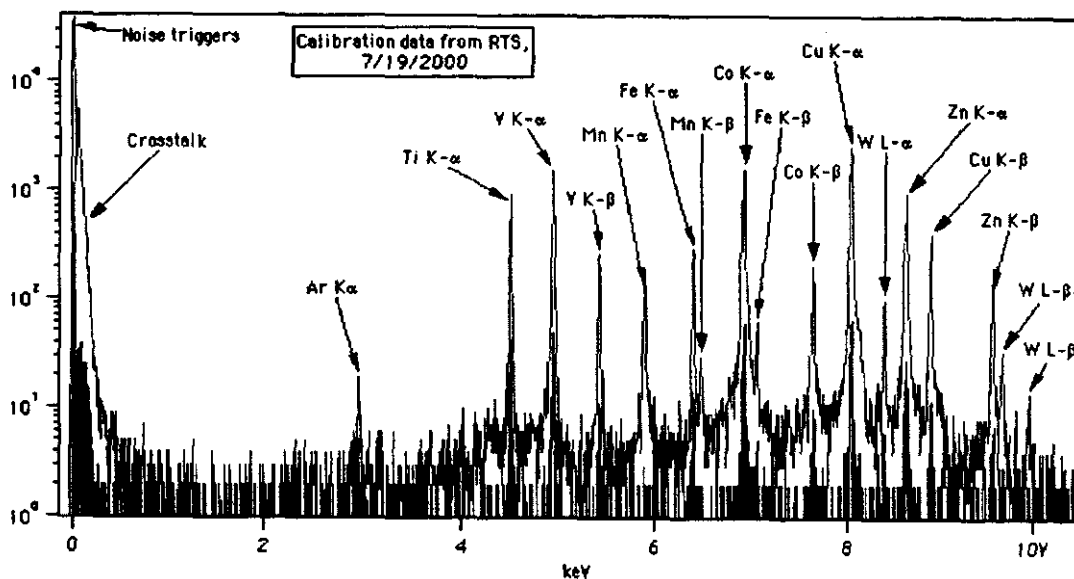


Figure 5. Calibration spectrum from the full co-added 32 pixel array using a rotating target fluorescence source. The darker spectrum underneath is that for a single pixel.

Transmission function of XRS/EBIT filter stack

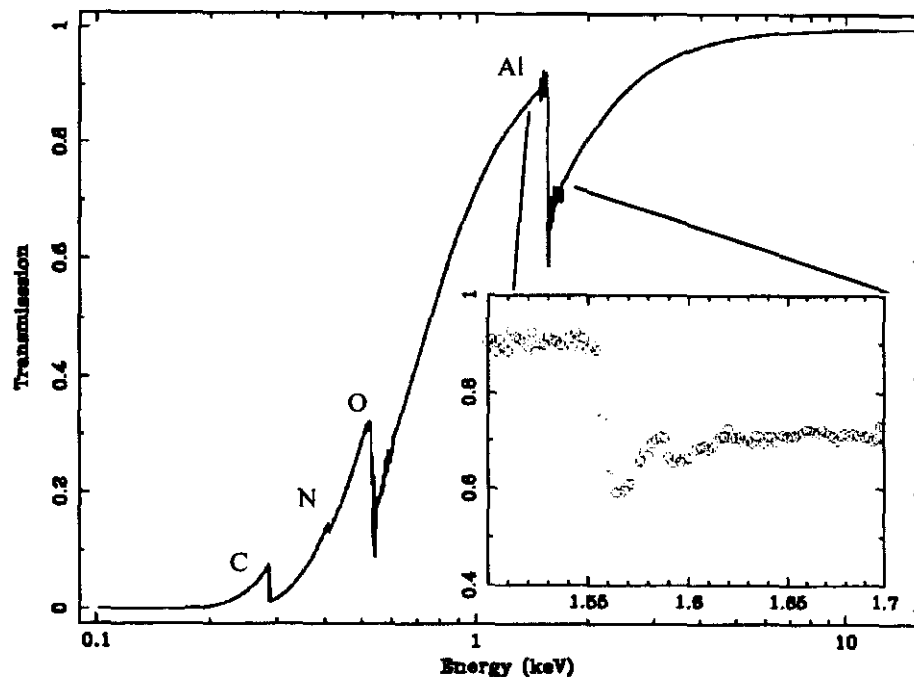


Figure 6. Filter transmission of the XRS/EBIT filter stack. The thickness of the polyimide and aluminum were determined by measuring the oxygen and aluminum edge structures using a variable spaced grating spectrometer. Inset is the measured extended fine structure of the aluminum K edge.

The in-situ measurement was done by attaching a Manson x-ray source with a Au target on a 12 foot beam line to the vacuum port on the XRS/EBIT. The long beam line is necessary because the Manson source is too bright for the XRS/EBIT

instrument. This continuum x-ray source evenly illuminates the microcalorimeter array and the depth of the oxygen and aluminum edges can be easily measured. The depth of the aluminum edge tells us whether the entire filter stack is intact and the depth of the oxygen edge compared to the offline measurements tells us about ice accumulation. Measurements after a 3 day pumpdown and 2 days at its base temperature indicate an additional $20 \mu\text{g}/\text{cm}^2$ of oxygen on the filters compared to about 10 for the filters themselves. This is well within our operating parameters. The ice accumulation is almost certainly from outgassing of the MLI insulation used in the cryostat. Periodic re-measurement of the oxygen edge will allow us to make corrections to the response function for the instrument. Experience with our sounding rocket instrument shows that the outgassing is minimal after the first few days at low temperatures.

4. PRELIMINARY RESULTS

Here we present some of the early results from our current observation campaign with the EBIT. The data are still not fully analyzed and the effects of the response function have not been included. We do not try to place much interpretation on the data beyond identifying spectral features. The interpretation of the results is ongoing and should yield exciting results in the near future.

4.1 Fe K and L shell emission for a monoenergetic electron beam

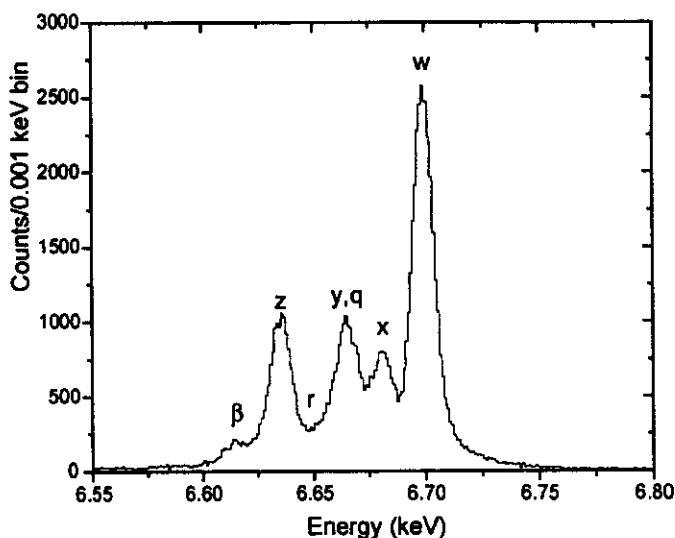


Figure 7. K shell emission spectrum of Fe XXV (He-Like) using the XRS/EBIT microcalorimeter detector. The resolution of the detector is about 11.5 eV FWHM.

For this experiment the EBIT machine is run in its monoenergetic mode without sweeping the electron beam energy. The calorimeter accumulates time and phase resolved x-ray events and then is able to fold them to remove the injection time. Figure 7 shows a spectrum of Fe K shell emission from Fe XXV (He-like) a small amount of Fe XXIV (Li-like) using the XRS/EBIT for an 18ks exposure. The individual lines in the He-like system are clearly resolved in the spectrum with very high statistics. The data were taken simultaneously with two Von Hamos style curved crystal spectrometers and the analysis of the relative line strengths will be combined between the three instruments.

Figure 8 shows an Fe L shell spectrum from charge states of Fe including Fe XXIII and Fe XXIV from both the calorimeter and a simultaneous measurement with a flat crystal spectrometer. It is clear from these observations that the instruments are very complementary. The crystal spectrometer has a resolution of about 1 eV but has a restricted bandpass and lower statistics. The calorimeter has much higher statistics and covers the entire band simultaneously. From figure 8 one can see that the crystal spectrometer clearly separates emission lines that form a blend in the calorimeter. We continue to survey the important Fe L shell emission for various charge states of Fe with the calorimeter and simultaneously with three crystal spectrometers.

The monoenergetic electron beam in the EBIT allows one to make single charge states of Fe. For example, at 1.75 keV electron energy, Fe XXII (C-like) is by far the dominant species. At 1.9 keV, Fe XXIII (B-like) takes over and accounts for the bulk of the emission. Thus by stepping through in beam energy it is possible to survey the steady state emission from each charge state for each ion species.

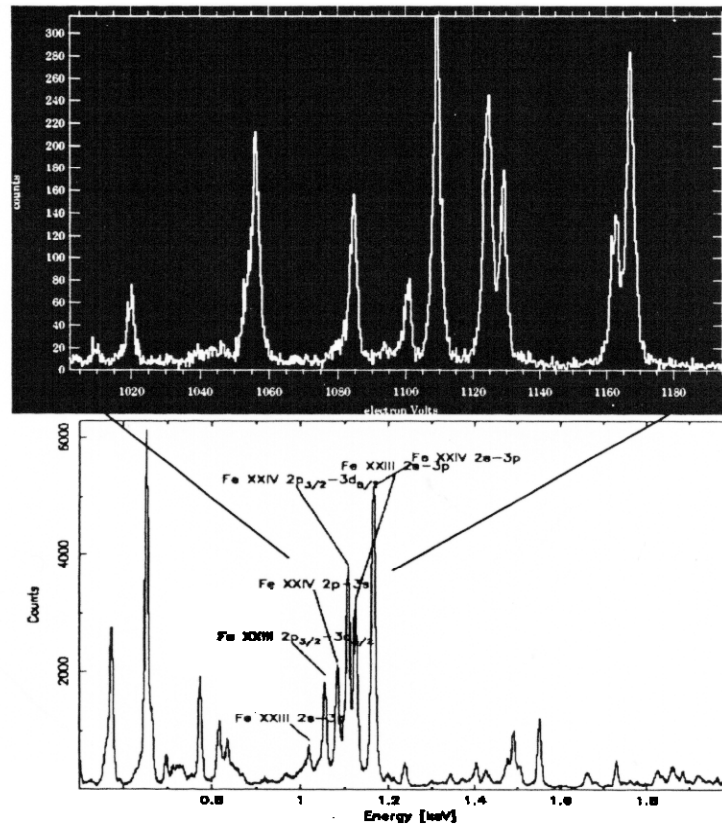


Figure 8. The lower panel is an L shell spectrum of Fe XXIII and XXIV along with K shell oxygen and other residual gas obtained with the EBIT/XRS microcalorimeter. The upper panel is a vacuum flat crystal spectrometer spectrum over its much narrower band pass. Note that the instruments are complementary. The crystal spectrometer helps split the line blends in the calorimeter spectrum.

4.2 Phase resolved spectroscopy, non-equilibrium plasmas

The EBIT machine runs in a continuous cycle of low charge state ion injection, ion trapping and then ion dumping to refresh the trap. The cycle is typically repeated every few seconds. When the ions are initially injected from the source (a metal vapor arc in the case of Fe) they are approximately singly charged. They are then ionized and collisionally excited by the electron beam. However, it takes a finite time for the ions to come into an equilibrium charge state where recombination balances ionization. During this time the ions charge up to higher states of ionization. For Fe this takes about 0.5 seconds. During this time the emission can be very bright compared to the equilibrium value. Thus if one is interested in looking at the steady state one must cut out the first half second of each multi-second cycle. We do this with the XRS/EBIT by phase folding the time stamped events with an injection trigger received from the EBIT as discussed in section 2. However, one can also look at the non-equilibrium plasma by making short phase cuts on the time after injection.

Figure 9 shows the power of the phase folding technique. Here we show 3 different phase cuts 5 ms long at 10ms, 100ms, and 500 ms after injection. The 500 ms panel represents the steady state ionization for a 2.3 keV monoenergetic beam. In Figure 9 one can clearly see the ionizing up of Fe from relatively low charge states up through its steady state value of predominately Fe XXIV. We have done more than 100 phase cuts, in 5 ms steps, on this data and can study in detail the time resolved evolution of a non-equilibrium plasma. The study of non-equilibrium plasmas is particularly important for understanding the emission at and behind shock fronts in objects such as supernova remnants¹⁷. The phase resolved measurements also enable us to pin point the time after which equilibrium has been reached, and allows us to cut out data that may adversely affect the excitation studies requiring equilibrium.

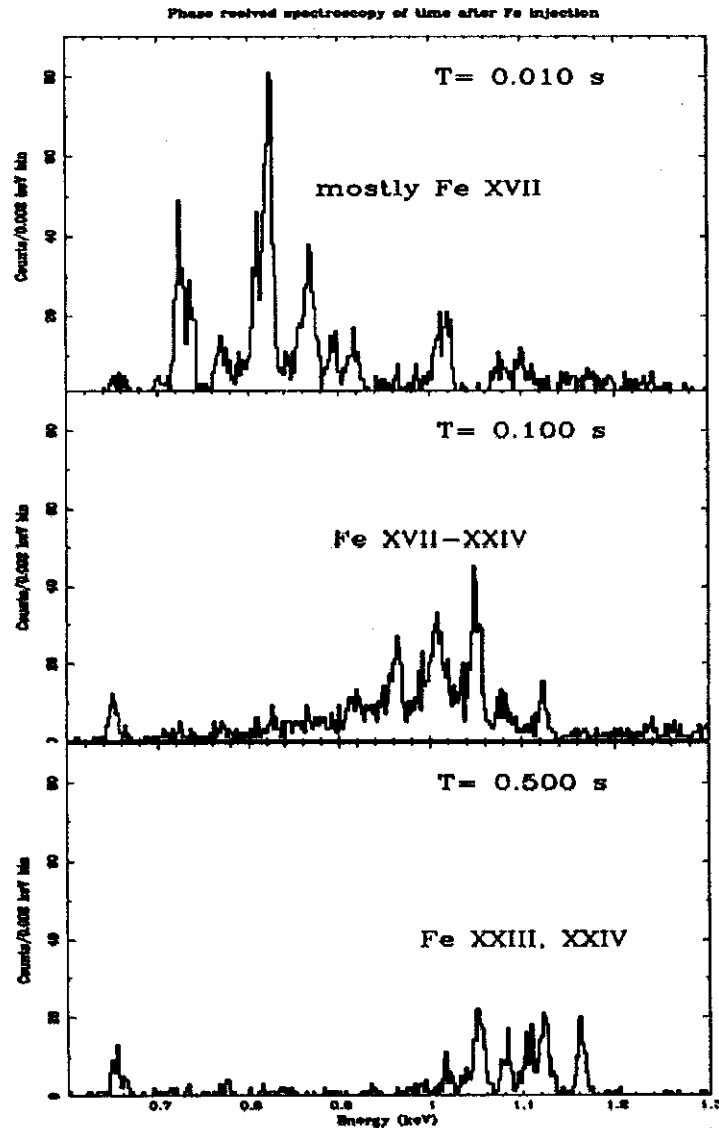


Figure 9. Phase folded spectrum of a non-equilibrium plasma. Three 5 ms long time slices are shown 10, 100, and 500 ms after Fe injection. The electron beam energy is 2.2 keV which will produce predominately Fe XXIII and XXIV as shown in the lower panel.

4.3 Maxwellian electron distributions in equilibrium plasmas

In addition to looking at collisional excitation from a monoenergetic electron beam, the EBIT machine is capable of scanning the electron beam energy on a fast time scale. The beam energy is ramped along a Maxwellian velocity profile very quickly compared to the injection period. Thus the ions quickly reach a steady ionization state, since recombination is a slow process, but with a Maxwellian velocity profile of the electrons. This allows the machine to closely approximate a plasma in collisional equilibrium with electrons at a single temperature. A beam profile is shown in Figure 10 for an electron temperature of $\langle kT \rangle = 2$ keV. In its current configuration the EBIT is capable of producing Maxwellian distributions over a broad range of temperatures up to about 3.5 keV. The upper limit is restricted by the ~ 24 keV maximum beam energy necessary to reproduce the tails of the distribution. In Figure 11 we show a spectrum of a Maxwellian distribution at $\langle kT \rangle = 2.2$ keV using the XRS/EBIT calorimeter. With this process we can simulate, for example, the conditions within an x-ray emitting cluster of galaxies at many different temperatures, an important topic in x-ray astrophysics.

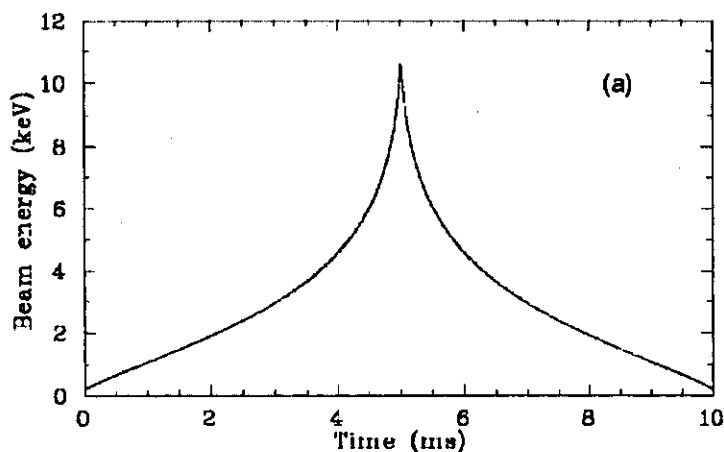


Figure 10. Electron beam energy profile to produce a Maxwellian velocity distribution. $\langle kT \rangle = 2.0$ keV in this example.

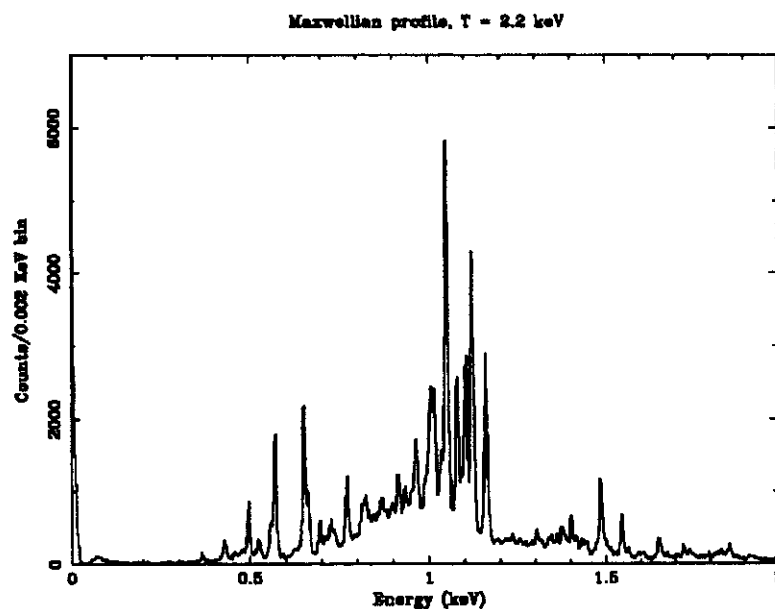


Figure 11. XRS/EBIT spectrum of a Maxwellian Fe plasma with $\langle kT \rangle = 2.2$ keV. Note that there are a large number of Fe L shell emission lines representing charge states from Fe XVII – Fe XXIV.

5. CONCLUSIONS

The XRS/EBIT instrument is based on a 6x6 square planar array of microcalorimeter detectors with 32 instrumented channels. The detectors are operated at 60 mK using an adiabatic demagnetization refrigerator in a portable laboratory cryostat. We have fully instrumented the cryostat with a complete set of XRS electronics that is capable of autonomously acquiring and processing x-ray events. We have successfully mated this instrument with the electron beam ion trap at Lawrence Livermore National Laboratory and it is currently running continuously. We have completed a large number of observations during the first two weeks of operation with this instrument including Fe K and L shell emission from several charge states, Fe with Maxwellian electron distributions, and phase resolved spectroscopy of non-equilibrium Fe plasmas. This is only a small sampling of the experiments completed to date and a great deal of analysis and interpretation has yet to be completed.

We have also completed an extensive calibration program that will allow us to create a detailed response function for the instrument. This is a necessary component to doing any sort of broadband relative flux measurements using our instrument. Line strength ratios are one of the key benefits of using the XRS/EBIT instrument but without extensive calibration and thus having a good handle on the uncertainties, it would be difficult to achieve definitive results.

We will continue to operate the instrument over the short term (weeks to months) but hope to design and build a more optimized instrument for permanent use at the EBIT facility at LLNL.

ACKNOWLEDGEMENTS

The authors wish to thank the many people at the Lawrence Livermore National Laboratory and at the NASA/Goddard Space Flight Center who worked on this project and on the XRS on Astro-E, without whom this experiment would not have been possible. In addition we thank Dan McCammon and Harvey Moseley for extensive help in conceiving and producing the XRS/EBIT over the last 15 years.

Work performed under the auspices of the U.S. D.o.E. by The University of California Lawrence Livermore National Laboratory under contract W-7405-ENG-48 and both the NASA/GSFC and LLNL components were supported by the NASA Space Astrophysics Research and Analysis Program.

REFERENCES

1. R. Kelley et al., "The Astro-E High Resolution X-Ray Spectrometer," *Proc. SPIE*, **3745**, p. 114, 1999.
2. P. Beiersdorfer, G. V. Brown, H. Chen, M.-F. Gu, S. M. Kahn, J. K. Lepson, D. W. Savin, and S. B. Utter, "Laboratory Data for X-Ray Astronomy," *Atomic Data Needs for S-Ray Astronomy*, ed. by M. B. Bautista, T. R. Kallman, and A. K. Pradhan, (<http://heasarc.gsfc.nasa.gov/docs/heasarc/atomic>), pp 103-116, 2000.
3. P. Beiersdorfer, G. V. Brown, J. J. Drake, M.-F. Gu, S. M. Kahn, J. K. Lepson, D. A. Liedahl, C. W. Mauche, S. B. Utter, and B. J. Wargelin, "Line Emission Spectra from Low-Density Laboratory Plasmas," *Revista Mexicana de Astronomia y Astrofisica* **9**, pp 123-130, 2000.
4. D. W. Savin, B. Beck, P. Beiersdorfer, S. M. Kahn, G. V. Brown, M. F. Gu, D. A. Liedahl, and J. H. Scofield, "Simulation of a Maxwellian Plasma Using an Electron Beam Ion Trap," *Physica Scripta* **T80**, pp 312-313, 1999.
5. G. V. Brown, P. Beiersdorfer, D. A. Liedahl, K. Widmann, S. M. Kahn, "Laboratory Measurements and Identification of the Fe XVIII-XXIV L-Shell X-ray line emission," University of California Lawrence Livermore National Laboratory document # UCRL-JC-136647.
6. G. V. Brown, P. Beiersdorfer, D. A. Liedahl, K. Widmann, S. M. Kahn, "Laboratory measurements and modeling of the Fe XVII x-ray spectrum", *ApJ* **502**, pp 1015-1026, 1998.
7. C. K. Stahle, D. McCammon, and K.D. Irwin, "Quantum Calorimetry," *Physics Today* **52**, p. 32, 1999.
8. C. K. Stahle et al., "Design and performance of the Astro-E/XRS microcalorimeter array and anti-coincidence detector," *Proc. SPIE* **3765**, p. 128, 1999.
9. F. S. Poter et al., "The Detector Assembly and the Ultra Low Temperature Refrigerator for XRS," *Proc. SPIE* **3765**, p. 729, 1999.
10. K. R. Boyce et al., "Design and Performance of the Astro-E/XRS Signal Processing," *Proc. SPIE* **3765**, p. 741, 1999.
11. M. A. Levine et al., *Nucl. Instrum. and Meth.* **B43**, p. 431, 1989.
12. G. V. Brown, P. Beiersdorfer, and K. Widmann, "Wide-band, High-Resolution Soft X-Ray Spectrometer for the Electron Beam Ion Trap," *Review of Scientific Instruments* **70**, pp. 280-283, 1999.
13. P. Beiersdorfer, R. Marrs, J. Henderson, D. Knapp, M. Levine, D. Platt, M. Schneider, D. Vogel, and K. Wong, "High-Resolution X-Ray Spectrometer for an Electron Beam Ion Trap," *Rev. Sci. Instrum.* **61**, pp. 2338-2342, 1990.
14. P. Beiersdorfer, J. R. Crespo López-Urrutia, P. Springer, S. B. Utter, and K. L. Wong, "Spectroscopy in the Extreme Ultraviolet on an Electron Beam Ion Trap," *Review of Scientific Instruments* **70**, pp 276-279, 1999.
15. K. C. Gendreau et al., "The Astro-E/XRS Calibration Program and Results," *Proc. SPIE* **3765**, p. 137, 1999.
16. M. D. Audley, et al., "Astro-E/XRS Blocking Filter Calibration," *Proc. SPIE* **3765**, p. 751, 1999.
17. see for example, R. Mewe and J. Schrijver, *Astronomy and Astrophysics* **87**, p.261, 1980, and V. Decaux, P. Beiersdorfer, S. M. Kahn, and V. L. Jacobs, "High-Resolution Measurement of the Ka Spectrum of Fe XXV to Fe XVIII: New Spectral Diagnostics of Non-Equilibrium Astrophysical Plasmas," *ApJ* **482**, pp 1076-1084, 1997.